Paper479

Magnetic Guidewire Control without Tip-Angle Detection in Sharply Curved Blood Vessel

Jayoung Kim, Byungjeon Kang
Robot Research Initiative
Medical Microrobot Center
Gwangju, Korea
Jaya@jnu.ac.kr, bjkang8204@jnu.ac.kr

Phu Bao Nguyen, Eunpyo Choi, Chang-Sei Kim*, Jong-Oh Park*
School of Mechanical Engineering
Chonnam National University
Gwangju, Korea
ckim@jnu.ac.kr, jop@jnu.ac.kr

***Abstract*—This paper proposes a position control algorithm for a magnetic guidewire without detection of tip-angle in sharply curved blood vessels. Key element of the proposed tip positioning control is to track a desired path regenerated in a blood vessel by a feeding control and an electromagnetic actuation (EMA) control. The path-regeneration creates an improved path in terms of properties of a magnetic guidewire and the size of a blood vessel when a magnetic guidewire can not traverse an original path. Based on a desired path, the feeding device and the EMA system make the translational and the rotational motion of a magnet tip, respectively. In this paper, for the EMA system, one pair of Helmholtz coil is employed to steer the magnet tip by adjusting the direction of the magnetic field. For the positioning control, a magnet tip is controlled with a regenerated path in order to follow a desired path without information of tip orientation. The proposed control methodology was verified through experiments on a phantom of sharply curved blood vessels. The experimental results proved that the proposed method could overcome the sharply curved blood vessel by control of the tip position of the guidewire with high accuracy in real-time.**

***Index Terms*—Magnetic Guidewire, Position Control, Path Regeneration, Minimum Contact**

I. Introduction

Over recent years, cardiovascular diseases have caused great concern since they became the biggest killer of adults in the world. In the medical field, there are various treatments in order to relieve suffering from the cardiovascular diseases such as catheter ablation (CA), percutaneous coronary intervention (PCI) and transcatheter aortic valve implantation (TAVI). In particular, PCI can be widely employed with various types of catheters with cardiovascular stents and balloons. During the procedure of PCI, cardiologists choose proper guidewire type in terms of the tip shape and the wire diameter depending on width of the ascending aorta, location of the coronary artery opening and direction of the proximal coronary artery. The effectiveness of PCI relies on treatment proficiency of a cardiologist in the selection of the guidewire type [1]. And cardiologists employ a X-ray fluoroscope and a contrast medium in order to recognize tip position of a guidewire and shape of a blood vessel in real time, respectively. X-ray fluoroscopes release harmful radiation and cardiologists are exposed to the radiation.

To solve the issues, many researchers have developed magnetically steerable catheter (MSC) systems which are able to operate on patient remotely and automatically. In the system of MSC, a magnet tip can be aligned along the direction of the magnetic field and the steering motion of a catheter can be derived by changing the orientation of the magnetic field. For such steering motion of a magnetic catheter, Epoch system (Stereotaxis) uses two motorized permanent magnets positioned on each side of the patient's body to make a uniform magnetic field inside the body [2] - [4]. However, the steerable motion in Epoch system is limited due to low response time and narrow permissible angle in rotation control of the permanent magnet. As another approach, CGCI (Magnetecs) [2] - [4] and Aeon (ETH) [4] - [5] employ multiple solenoid coils with a paramagnetic core, such as 8 or 7 electromagnetic coils respectively, to obtain muti-degree of freedom of a catheter tip for cardiac ablation. They generate the uniform as well as the gradient magnetic field and control the 3-dimensional motions of a magnetic catheter inside the patient's chest.

In the related systems, a real-time technique of catheter detection is required for the catheter control to acquire position and angle of a catheter tip by a X-ray fluoroscope with a contrast medium [6]. However, it is more difficult to recognize the tip angle if the magnet tip and the wire diameter become much smaller and thinner for micro-invasion, respectively. Therefore, this paper is focused on a tip positioning control without detection of the tip angle, which can overcome sharply curved blood vessels with minimum surface contact of the catheter tip. And also, this paper uses one pair of Helmholtz coil in consideration of the way to reduce the number of coils for 2-dimensional motion on x-y plane instead of two pairs of Helmholtz coil in our previous paper [7].

II. Magnetic Guidewire System and Motion

Main components of a magnetic guidewire system are an electromagnetic actuator (EMA), a feeding device and a magnetic guidewire. The EMA system consists of one pair of Helmholtz coil which can generate the uniform magnetic field of Helmholtz coil on x-y plane as shown in Fig. 1. Radius and wire turns of the coils are 162 mm and 494, respectively. The Region of interest (ROI) is 10 cm $\times$ 10 cm square and the phantom of blood vessels is placed on the center of the EMA system. The magnetic guidewire is composed of a 0.2 mm (D) Nitinol wire and a 2 mm (D) x 2 mm (H) cylindrical magnet (NdFeB). And the magnet is attached to the wire-tip point as shown at the upper center box of Fig. 1. The feeding device controls the velocity and the displacement of the magnetic guidewire during insertion and retrieval motion in the blood vessel.

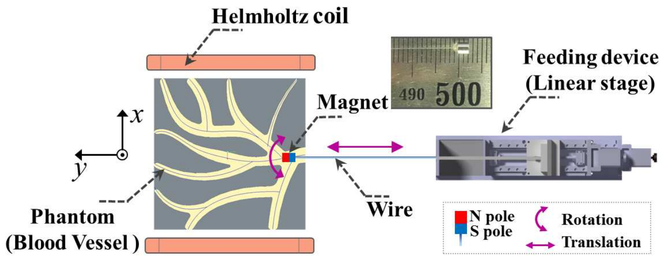

Fig. 1. Components of the magnetic guidewire system (MGS)

The magnetic guidewire motion can be derived by two actuation systems of the feeding and the EMA system. The feeding system can make a translational motion of the magnet tip with the feeding velocity V_F for insertion and retrieval of the guidewire. And the EMA system can make a rotational motion of the magnet tip by aligning the uniform magnetic field into a desired direction. From Maxwell's equation, torque **T** of a magnet is generated by an electromagnetic field **B** as follows:

$$\mathbf{T} = V\mathbf{M} \times \mathbf{B} \tag{1}$$

where V and **M** denote the volume and magnetization of the magnet, respectively. Initially, the magnetic guidewire is situated on y-axis and the magnetization **M** is given as:

$$\mathbf{M} = \begin{bmatrix} M_x \\ M_y \\ M_z \end{bmatrix} = \begin{bmatrix} M cos(\alpha) \\ M sin(\alpha) \\ 0 \end{bmatrix} \tag{2}$$

And this paper uses only one pair of Helmholtz coil placed on x-axis. Accordingly the magnetic flux of the magnetic field **B** can be expressed in (3).

$$\mathbf{B} = \begin{bmatrix} B_x \\ B_y \\ B_z \end{bmatrix} = \begin{bmatrix} B_x \\ 0 \\ 0 \end{bmatrix} \tag{3}$$

And the magnetic flux on x-axis is derived by giving current i to the Helmholtz coils as follows:

$$\begin{aligned} B_x = \frac{iNR_H^2}{2}[(R_H^2 + (\frac{R_H}{2} - x_H)^2)^{-3/2} \\ +(R_H^2 + (\frac{R_H}{2} + x_H)^2)^{-3/2}] \end{aligned} \tag{4}$$

where N is the coil turns, R_H is the radius of coils and x_H is the x-axis position from the center point of each Helmholtz coil. From (1), (2) and (3), therefore, magnet torque T_m of the guidewire tip can be expressed as:

$$T_m = -VB_xM_y = -VB_xMsin(\alpha) \tag{5}$$

Once the magnetic field is exerted on the magnet, the magnet tip can be rotated by the magnet torque T_m as shown in Fig. 2. By the steering motion, the steering angle ϕ can be defined as the equation of the wire deflection in (6).

$$\phi = \frac{T_m l_w}{EI} \tag{6}$$

where E, I and l_w are the elastic modulus, the moment of inertia and the wire length, respectively.

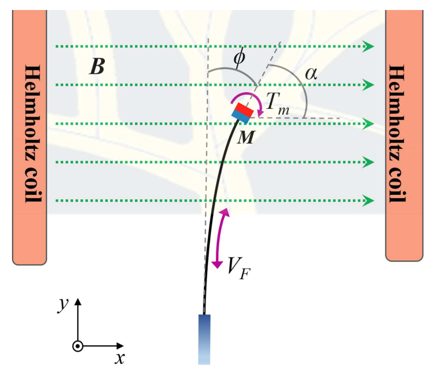

Fig. 2. Motion of a magnetic steering guidewire

III. Tip Positioning Control

The proposed tip-positioning control of the magnetic guidewire can be largely categorized into three topics as depicted in Fig. 3; **1)** Path-regeneration, **2)** Feeding control, **3)** EMA control. In the control, the key algorithm is the path-regeneration with the feeding and EMA control and it can have the magnetic guidewire to make minimum contact with the inner surface of a blood vessel while following a desired path, simultaneously. The path-regeneration draws an improved path in terms of properties of the guidewire and the size of the blood vessel at the current position of the magnet tip when the guidewire can not traverse the original path generated by the path-generator in advance. The feeding control is based on the E-equation which acts as the weight factor to enhance the tip-positioning performance. In the feeding control, the desired feeding velocity is initially selected as V_{Fd} and the translational motion of the guidewire is controlled by the feeding device with the control input u_F according to the distance error e_D. The EMA control is based on conventional PID control and it employs the position error e_P for the feedback information. The rotational motion of the guidewire is derived by the control input u_E depending on the position error e_P. For actual tip position P_{tip} should be recognized in real time using the vision tracking algorithm which is constructed in the loop of the proposed control. But the contents regarding the vision tracking was omitted from this paper.

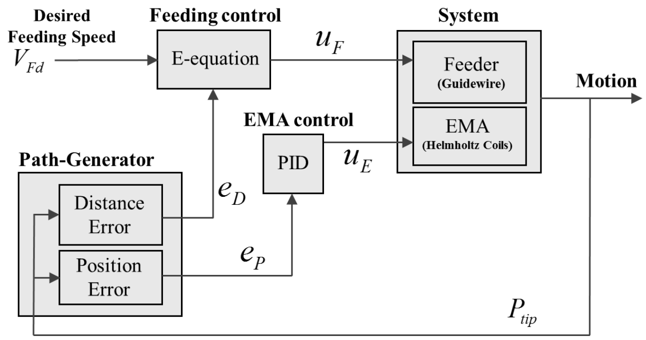

Fig. 3. Schematic diagram of proposed tip positioning control

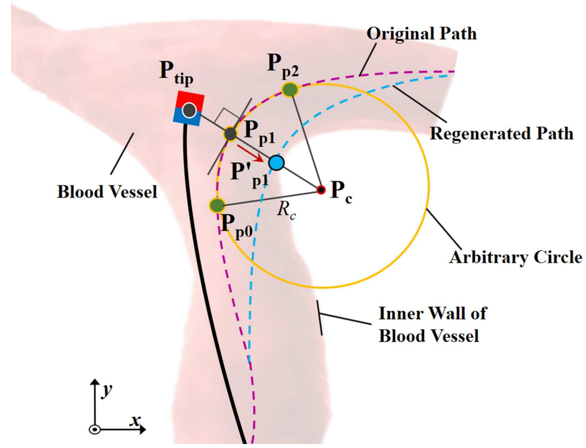

Fig. 4. Path replanning by permissible radius of curvature

A. Path Regeneration

The path-regeneration evaluates the radius of curvature of the original path in order to determine whether to regenerate the path or not. The radius of curvature plays an important role on path-following performance. The path curvature can be derived from the radius of curvature and if the curvature is higher than the permissible bending angle of the magnetic catheter, the catheter can not overcome the path in a sharply curved blood vessel. To calculate the radius of curvature, first of all, three points on the original path can be selected based on the *x* and *y* position of the magnetic tip. In Fig. 4, $\mathbf{P_{p1}}$ on the original path is the closest point to the current position $\mathbf{P_{tip}}$ of the magnet tip. And also, $\mathbf{P_{p0}}$ and $\mathbf{P_{p2}}$ on the original path are the previous point and the next point from $\mathbf{P_{p1}}$, respectively. Hence, the radius of curvature R_c can be obtained from the circle equation with the three points of $\mathbf{P_{p0}}$, $\mathbf{P_{p1}}$ and $\mathbf{P_{p2}}$ as follows:

$$R_c = \|\mathbf{P_c} - \mathbf{P_{p0}}\| = \|\mathbf{P_c} - \mathbf{P_{p1}}\| = \|\mathbf{P_c} - \mathbf{P_{p2}}\| \tag{7}$$

where $\mathbf{P_c}$ is the center point of the circle. To complete the circle equation, the elements of each point in (8) are substituted into (7) and then the equation with respect to the center point of the circle $\mathbf{P_c}$ can be derived as (9).

$$\begin{aligned} \mathbf{P_c} &= (x_c, y_c), \quad & \mathbf{P_{p0}} &= (x_0, y_0) \\ \mathbf{P_{p1}} &= (x_1, y_1), \quad & \mathbf{P_{p2}} &= (x_2, y_2) \end{aligned} \tag{8}$$

$$\mathbf{A_1 P_c} = \mathbf{A_2} \qquad \rightarrow \qquad \mathbf{P_c} = \mathbf{A_1^+ A_2} \tag{9}$$

where superscript $^+$ indicates a pseudoinverse and each matrix in (9) can be arranged into (10). Accordingly, the calculated $\mathbf{P}_c$ is used for obtaining the radius of curvature R_c by substituting $\mathbf{P}_c$ into (7).

$$\mathbf{A_1} = \begin{bmatrix} -2x_0 + 2x_1 & -2y_0 + 2y_1 \\ -2x_1 + 2x_2 & -2y_1 + 2y_2 \\ -2x_0 + 2x_2 & -2y_0 + 2y_2 \end{bmatrix}$$
$$\mathbf{A_2} = \begin{bmatrix} -x_0^2 - y_0^2 + x_1^2 + y_1^2 \\ -x_1^2 - y_1^2 + x_2^2 + y_2^2 \\ -x_0^2 - y_0^2 + x_2^2 + y_2^2 \end{bmatrix}$$
$$\mathbf{P_c} = \begin{bmatrix} x_c \\ y_c \end{bmatrix} \tag{10}$$

To evaluate the possibility of following the path, R_c derived from (7) is compared with the permissible radius of curvature R_{cLimit} as depicted in Fig. 5. First of all, for R_{cLimit}, the permissible steering angle ϕ_{Limit} is derived by the maximum magnet torque T'_m in (11) based on the equation of the wire deflection as (12). The maximum magnet torque T'_m is conservatively redefined from (5) by assuming that the magnetic flux B_x is maximally exerted on the magnet tip and the angle of the sharply curved path is closed to $\pi/2$.

$$T'_m = VB_{x_{max}}M_y \tag{11}$$

$$\phi_{Limit} = \frac{T'_m l_w}{EI} \tag{12}$$

In Fig. 5, ϕ_{Limit} is the included angle between the $\mathbf{P_{p1}}$-$\mathbf{P_{p0}}$ line and $\mathbf{P_{p2}}$-$\mathbf{P_{p0}}$ line. In the triangle of $\triangle\mathbf{P_{p0}P_{p1}P_{p2}}$, the angles of $\angle\mathbf{P_{p1}P_{p0}P_{p2}}$ and $\angle\mathbf{P_{p1}P_{p2}P_{p0}}$ indicate the permissible steering angle ϕ_{Limit}. Accordingly, the angle θ_{Limit} of $\angle\mathbf{P_{p0}P_{p1}P_{p2}}$ can be obtained by (13).

$$\theta_{Limit} = \pi - 2\phi_{Limit} \tag{13}$$

From (13), the permissible radius of curvature R_{cLimit} can be derived using the second law of cosines in $\triangle\mathbf{P_{p0}P_{p1}P_c}$ as follows:

$$R^2_{c_{Limit}} = R^2_{c_{Limit}} + l_p^2 - 2R_{c_{Limit}} l_p cos(\frac{\theta_{Limit}}{2}) \tag{14}$$

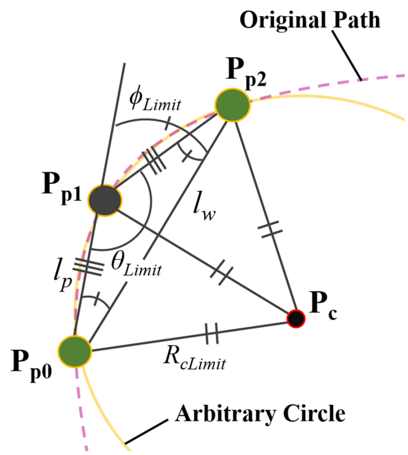

Fig. 5. limit condition of the radius of curvature

$$R_{c_{Limit}} = l_p / \{2cos(\frac{\theta_{Limit}}{2})\} \tag{15}$$

where l_p is the distance between $\mathbf{P_{p0}}$ and $\mathbf{P_{p1}}$. The permissible radius of curvature R_{cLimit} is considered in correlation with the properties of the guidewire and the original path. Hence, the radius of path curvature R_c can be compared with R_{cLimit} to evaluate the possibility of the magnetic guidewire for following the path. If R_c is less than or equal to R_{cLimit}, then the original point $\mathbf{P_{p1}}$ is recalculated as $\mathbf{P'_{p1}}$ which is the closest point to the corner of inner wall in a blood vessel. $\mathbf{P'_{p1}}$ is placed on the $\mathbf{P_{p1}}$-$\mathbf{P_c}$ line as shown in Fig. 4.

$$\textit{If} \quad R_c \leq R_{c_{Limit}}, \quad \textit{then} \quad \mathbf{P_{p1}} \quad \Rightarrow \quad \mathbf{P'_{p1}} \tag{16}$$

In this paper, the desired path is generated using the cubic spline equation. The cubic spline curve contains the control points which can change the curvature of the path. Therefore, $\mathbf{P'_{p1}}$ is employed to redraw the spline curve as the new control point on the path. In Fig. 4, the blue-dashed line is the regenerated path by $\mathbf{P'_{p1}}$ and it results in the decreased angle than the original path (the red-dashed line) to pass through the desired blood vessel.

B. Tip Positioning Methodology

For positioning the magnetic guidewire, this paper focuses on two types of controls for the rotational and the translational motion using the EMA system and the feeding device, respectively. In the control loop of Fig. 3, the position error e_P is employed to rotate the magnetic tip toward the desired point on the given path by adjusting the magnetic flux B_x generated by the EMA system and the distance error e_D is considered in order to make the translational motion of the guidewire by changing the feeding velocity in the feeding device. In the rotation control, the position error e_P is considered as one angle-based parameter which can determine the rotational direction of the magnet tip and the magnitude of the magnetic field, simultaneously. The position error e_P can be derived using the three points of $\mathbf{P_{tip}}$, $\mathbf{P_{p1}}$ and $\mathbf{P_{p2}}$ as shown in Fig. 6. First of all, the points of $\mathbf{P_{tip}}$ and $\mathbf{P_{p1}}$ on the global coordinate are transformed into the points of $\mathbf{P_{tip\text{-}p2}}$ and $\mathbf{P_{p1\text{-}p2}}$ on the $\mathbf{P_{p2}}$ coordinate, respectively, as (17).

$$\begin{aligned} \mathbf{P_{tip\text{-}p2}} &= \mathbf{P_{tip}} - \mathbf{P_{p2}} \\ \mathbf{P_{p1\text{-}p2}} &= \mathbf{P_{p1}} - \mathbf{P_{p2}} \end{aligned} \tag{17}$$

And the point of $\mathbf{P_{tip\text{-}p2}}$ can be matched with $\mathbf{P_{p1\text{-}p2}}$ by the rotation matrix $\mathbf{R_P}$ with the position error e_p in (18).

$$\mathbf{P_{p1\text{-}p2}} = \mathbf{R_P}\mathbf{P_{tip\text{-}p2}}, \quad \mathbf{R_P} = \begin{bmatrix} cos(e_P) & -sin(e_P) \\ sin(e_P) & cos(e_P) \end{bmatrix} \tag{18}$$

From (18), the matrix of the position error $\mathbf{D}$ is designed by newly arranging the matrix of the tip position $\mathbf{P_{tipN}}$ and $\mathbf{D}$ can be calculated by applying the pseudoinverse of $\mathbf{P_{tipN}}$ in (19).

$$\mathbf{P_{p1\text{-}p2}} = \mathbf{P_{tipN}}\mathbf{D} \qquad \Rightarrow \qquad \mathbf{D} = \mathbf{P^{+}_{tipN}}\mathbf{P_{p1\text{-}p2}} \tag{19}$$

$$\mathbf{D} = \begin{bmatrix} D_1 \\ D_2 \end{bmatrix} = \begin{bmatrix} sin(e_P) \\ cos(e_P) \end{bmatrix}, \quad \mathbf{P_{tipN}} = \begin{bmatrix} -y_{tip} & x_{tip} \\ x_{tip} & y_{tip} \end{bmatrix}$$

And the position error e_P is obtained by calculating the simple trigonometric function as follows:

$$e_P = tan^{-1}(\frac{D_1}{D_2}) \tag{20}$$

The position error e_P is applied for the EMA control into the conventional PID control for the rotational motion and the PID control law is given as:

$$u_E(t) = K_p e_P(t) + K_i \int e_P(t)dt + K_d \dot{e_P}(t) \tag{21}$$

where t is the sampling time, $u_E(t)$ is the control input at current step. K_p, K_i and K_d are the gains of the PID controller.

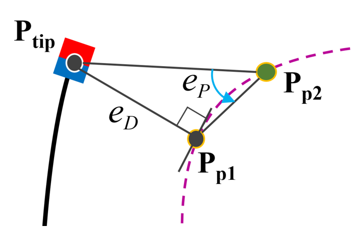

Fig. 6. Error calculation for the positioning control

For the translational motion, the feeding controller observes the distance error e_D in Fig. 6 which is the absolute distance between $\mathbf{P_{tip}}$ and $\mathbf{P_{p1}}$ as (22).

$$e_D = \|\mathbf{P_{tip}} - \mathbf{P_{p1}}\| \tag{22}$$

To control the feeding velocity, a theoretical form of the control input u_F can be designed as an exponential equation with the distance error e_D as follows:

$$u_F(t) = V_{Fd}(1 - e^{-\lambda/e_D(t)}) \tag{23}$$

where V_{Fd} is the desired feeding speed and λ is the feeding coefficient. λ can be selected in the allowable range of control accuracy. In (23), the control input u_F becomes the desired feeding speed V_{Fd} if the distance error e_D is in the range of the allowable distance error determined by the feeding coefficient λ. In this paper, the allowable distance error is 0.2 mm. In the case of more than 0.2 mm, the control input u_F is linearly changed into a low value less than V_{Fd} in order to keep the current position of the tip.

IV. Experimental Results

In the experimental environment, the wire diameter of the magnetic guidewire is 0.2 mm and it was made of Nitinol which has the elastic modulus (E) 40 GPa at human body temperature (37 °C) [8] - [9]. And the one pair of Helmholtz coil on x-axis was employed within maximum current 20 A of the power supply, which can generate 2182 A/m of the magnetic field. The experiments were carried out in the phantom which is composed of several types of the blood vessels as shown in Fig. 1. The blood vessels were constructed within the diameter between the maximum size 12 mm and minimum size 4 mm. And CCD camera was set up on the top of the system to detect the position of the magnet tip.

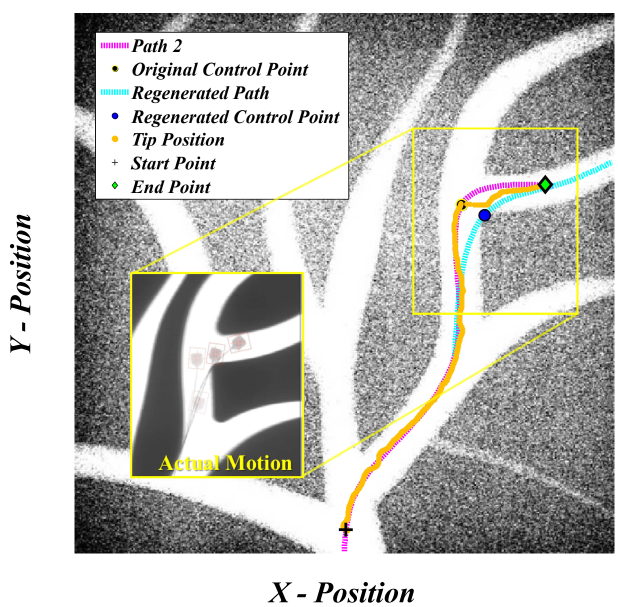

Fig. 7. Result of the positioning control on the desired path

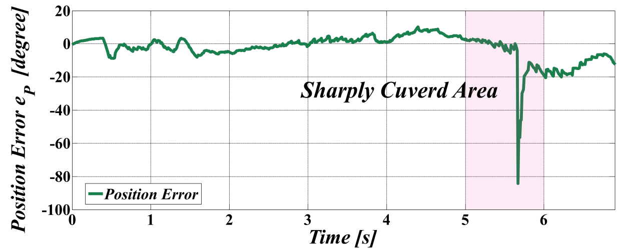

(a) Position error

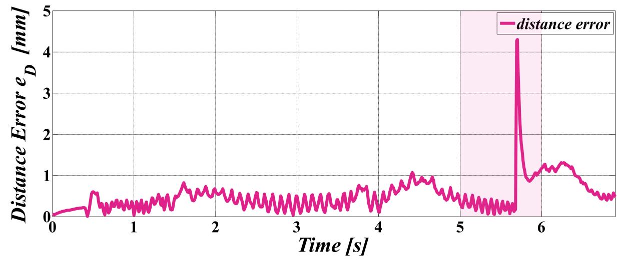

(b) Distance error

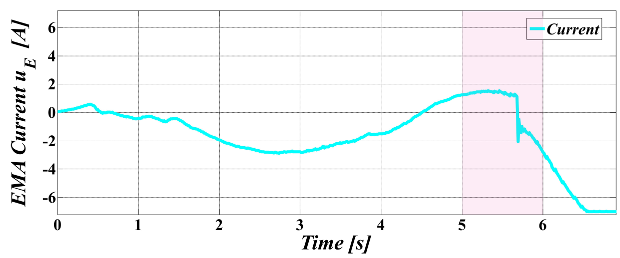

(c) EMA Current

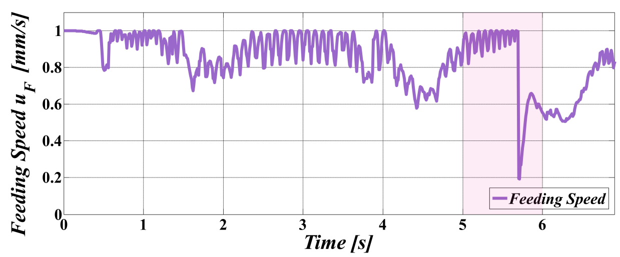

(d) Feeding velocity

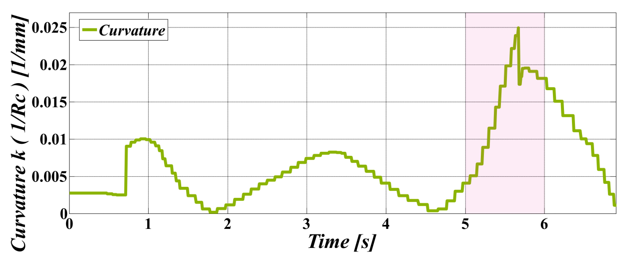

(e) Curvature

Fig. 8. Experimental data on the desired path

To validate the performance of the tip-positioning, sharply curved blood vessel in the phantom was selected to draw the desired path as depicted in Fig. 7. In the blood vessel, the original desired paths are initially generated by the cubic spline equation in advance and the magnetic guidewire system controls the magnet tip to make the rotational and the translational motions along the path with 10 Hz frequency of the control loop in real time. The experiments were conducted thee times on the path. The experiments were carried out to verify the control performance while the guidewire is inserted into the phantom. Fig. 7 shows the result of the positioning control in the blood vessel. From the start point +, the magnet tip precisely followed the original path before reaching the sharply curved region. At the sharply curved point (Original Control Point) on the original path, the regenerated control point was newly derived by the path regeneration and the magnet tip was focused on tracking the regenerated path to overcome the blood vessel. The yellow line is the actual position of the magnet tip and in the sharply curved area, the magnet tip tried to be matched with the regenerated path until arriving at the end point $\diamond$ as shown in Fig. 7. Actually, the tip motion was derived by following the regenerated path in order to pass through the blood vessel as shown in the left-side yellow box of Fig. 7.

From the results of the experiments, Fig. 8 numerically demonstrates the control performance of positioning the magnetic guidewire on the Path. The distance error e_D was less than about 1 mm during 5.6 s in (b) of Fig. 8 and the feeding speed was closed to the maximum velocity (the desired velocity V_F) 1 mm/s in (d) of Fig. 8. After that, the sharply curved point appeared at around 5.6 s and the values of all the graphs was drastically changed since the desired path was regenerated at that time. By the regenerated path, the position error e_P and the distance error e_D rapidly increased in (a) and (b) of Fig. 8. For positioning the magnet tip, the EMA system and the feeding device tried to exert much more change rate of the magnetic field to the magnet and to rapidly reduce the translational speed of the guidewire, respectively. In (e) of Fig. 8, the graph of the curvature *k* accounts for the advantage of the path regeneration. At 5.6 s, the curvature on the original path increased up to the permissible curvature ($1/R_{cLimit}$) 0.025 [1/mm]. After replanning the path, meanwhile, the curvature decreased until 0.017 [1/mm] at 5.6 s, which is able to become much smoother than the original path. That is the reason why the proposed positioning method can rotate the magnet tip only by detecting the position without tracking the orientation of the guidewire. To evaluate the accuracy of positioning the guidewire, root mean square (RMS) and standard deviation (STD) were used in 3 replicates on the blood vessel. RMS error and STD showed average 0.63($\pm$0.4) mm error. Therefore, the results proved that the proposed method could overcome the sharply curved blood vessel by control of the tip position of the guidewire with high accuracy in real-time.

V. Conclusion

This paper proposed the novel tip-positioning algorithm of the magnetic steerable guidewire for PCI treatment. In this paper, one pair of Helmholtz coil was employed to steer the magnet tip by adjusting the magnetic field. And the feeding device was applied to make the translational motion of the guidewire. In the positioning control, the magnet tip was controlled with minimum contact to the inner wall of the blood vessel by replanning the newly desired path instead of the information of the guidewire orientation. The proposed algorithm was verified through the control experiments on the sharply curved path and it could be validated from the accuracy evaluation of the results.

Acknowledgment

This research was supported by the Bio & Medical Technology Development Program of the National Research Foundation (NRF) funded by the Korean government (MSIT) (No. 2015M3D5A1065682).

References

[1] C. Walker, “Guide-wire selection for peripheral vascular interventions,” *Endovascular Today*, evtoday.com, 2013.

[2] Bich Lien Nguyen, Jose L Merino and Eli S Gang, “Remote Navigation for Ablation Procedures-A New Step Forward in the Treatment of Cardiac Arrhythmias,” *European Cardiology*, vol. 6, no. 3, pp. 50-56, 2010.

[3] Antoine Da Costa, Jean Baptiste Guichard, Cecile Romeyer-Bouchard Antoine Gerbay and Karl Isaaz, “Robotic magnetic navigation for ablation of human arrhythmias,” *Medical Devices: Evidence and Research*, vol. 9, pp. 331-339, 2016.

[4] Vi T.H. Le, “Accurate modelling and positioning of a magnetically-controlled catheter tip,” *Thesis: Masters in Edith Cowan University*, May 2015.

[5] Janis Edelmann, Andrew J Petruska and Bradley J Nelson, “Magnetic control of continuum devices,” *The International Journal of Robotics Research*, vol. 36, no. 1, pp. 68-85, 2016.

[6] Ping-Lin Chang, Alexander Rolls, Herbert De Praetere, Emmanuel Vander Poorten, Celia V Riga, Colin D. Bicknell and Danail Stoyanov, “Robust Catheter and Guidewire Tracking Using B-Spline Tube Model and Pixel-Wise Posteriors,” *IEEE Robotics and Automation Letters*, vol. 1, no. 1, pp. 303-308, January 2016.

[7] Semi Jeong, Hyunchul Choi, Gwangjun Go, Cheong Lee, Seong Young Ko, Jong-Oh Park and Sukho Park, “Feasibility Study on Magnetically Steerable Guidewire Device for Percutaneous Coronary Intervention,” *International Journal of Control, Automation and System*,vol. 15, no. 1, pp. 473-479, 2016.

[8] Helge Fischer-Brandies, Mohammed Es-Souni, Norman Kock, Klaus Raetzke, Ole Bock, “Transformation Behavior, Chemical Composition, Surface Topography and Bending Properties of Five Selected 0.016”x0.022” NiTi Archwires,” *Journal of Orofacial Orthopedics*, no. 2, pp. 88-99, November 2002.

[9] Marcelo do Amaral Ferreira, Marco Antonio Luersen, Paulo Cesar Borges, “Nikel-titanium alloys: A systematic review,” *Journal of Orthdontics*, vol. 17, no. 3, pp. 71-82, May 2012.